JOURNAL OF GEOPHYSICAL RESEARCH, VOL. 95, NO. B7, PAGES 11,283-l 1,292, JULY 10, 1990

Extracting Shear Wave Polarizations From Different Source Orientations: Synthetic Modelling

HEINER IGEL[1,2] AND STUART CRAMPIN
British Geological Survey, Edinburgh, Scotland

Shear wave splitting, diagnostic of some form of seismic anisotropy, has been identified in the past, principally by examining polarization diagrams and by rotating the axes of recordings to separate the shear wave polarizations. We introduce a new technique for identifying polarizations of shear waves when the data has been recorded with more than one source orientation. The technique, suitable for vertical seismic profiles (VSPs) or reflection data, averages over an entire shear wavetrain, eliminating source related effects while retaining the anisotropy related polarizations. In shear wave reflection experiments and shear wave VSPs the distribution of displacement directions depends on the elastic properties of the medium (anisotropy), the source orientation, and the effects of scattering. We linearly combine seismograms from different source polarizations in order to simulate seismograms for any source polarization. This allows us to show the distribution of displacement directions as a function of source polarization in a high-relief display. The diagrams show characteristic features in the presence of anisotropy which could help to determine the polarizations of the two split shear waves in difficult circumstances. The techniques are tested with synthetic seismograms.

1. INTRODUCTION

We examine the effects of source orientation on the distribution of polarization directions in the horizontal plane of near-offset shear wave vertical seismic profiles (VSPs) and reflection surveys. Processing seismograms from two different source orientations yields direct information about the shear wave splitting and allows the polarizations of the two split shear waves to be recognized even in the presence of considerable noise. This could be particularly useful if the delay between the split shear waves in field recordings is small, or if interference of many signals leads to elliptical particle motion, where it would be impossible to identify the polarization by examing individual three-component records.

In the absence of anisotropy, the observed polarization of shear waves should be those radiated from the source, modified only by interaction with internal interfaces and with the free-surface topography. The scattering of shear waves at a free surface has been discussed by *Nuttli* [1961, 1964], *Evans* [1984], and *Booth and Crampin* [1985]. They showed that shear waves observed at the free surface may be seriously distorted by interaction with the surface if the angle of incidence is greater than the critical angle arcsin (Vs/Vp). This angle defines a shear wave window, within which the shear waveforms recorded at the surface are similar to the waveforms of the incident waves.

The effects of internal interfaces and inhomogeneities have been discussed by *Cormier* [1984], *Douma and Helbig* [1987], and *Liu and Crampin* [this issue], Cormier concluded that interaction with irregular internal interfaces could lead to distortions of shear wave polarizations of up to 10°. *Douma and Helbig* [1987] suggested that interference with plane interfaces could have serious implications for the study of anisotropy-induced shear wave splitting. However, *Liu and Crampin* [this issue] show that, although interaction with single internal plane interfaces may contribute to the observed complexity of the waveforms following the initial onset of the faster split shear wave, the changes in orientation of the wave caused by the interface are small and only affect details of the behavior of the patterns in the polarization diagrams and not the initial takeoff angles.

Shear wave splitting-is caused by the internal structure of the rockmass along the raypath. The structure may be interfaces or discontinuities, but more commonly is some form of effective anisotropy *[Liu and Crampin,* this issue]. The visual identification of polarization directions of split shear waves by rotating record axes or by analyzing polarization diagrams may be difficult if the delay between the split shear waves is small because the anisotropy is weak, or the particle displacements are elliptical because of

[1]Also at Geophysikalisches Institut der Universität Karlsruhe, Federal Republic of Germany.
[2]Now at Institut de Physique du Globe, Paris, France.

Paper number 90JB00265.
0148-0227/90/90JB-00265$05.00

interference from reflected signals. The processing technique discussed in this paper allows the polarization directions of the split shear waves to be determined even in the case of strongly elliptical motion.

2. PRINCIPLE OF THE METHOD

We assume a minimum of two different shear wave VSP data sets recorded at the same well with different source azimuths, and consider near-vertical propagation. The ideas developed in this paper are valid for any offset and for planes of displacement approximately perpendicular to the propagation direction of the incident waves. Since we restrict ourselves to shear wave particle motion of nearly vertical ray paths, we will only consider the horizontal components of recorded motion. For a given shear wave source polarization θ, we take two fixed horizontal orthogonal directions in the medium with components of the recorded displacement vector $x(\theta, t)$, and $y(\theta, t)$, measured in the coordinate system in Figure 1. Let $x_1(t)$, $y_1(t)$ and $x_2(t)$, $y_2(t)$ be the displacements for two (different) source orientations θ_1, and θ_2, respectively.

When the two source orientations are perpendicular ($\theta_2 - \theta_1 = 90°$), the displacements become

$$\begin{aligned} x(\theta, t) &= \cos(\theta-\theta_1)\, x_1(t) + \sin(\theta-\theta_1)\, x_2(t) \\ y(\theta, t) &= \cos(\theta-\theta_1)\, y_1(t) + \sin(\theta-\theta_1)\, y_2(t) \end{aligned} \quad (1)$$

When $\theta_1 - \theta_2 \neq 90°$, we have

$$\begin{aligned} x(\theta, t) &= (\sin(\theta-\theta_2)/\sin(\theta_1-\theta_2))\, x_1(t) \\ &\quad - (\sin(\theta-\theta_1)/\sin(\theta_1-\theta_2))\, x_2(t) \\ y(\theta, t) &= (\sin(\theta-\theta_2)/\sin(\theta_1-\theta_2))\, y_1(t) \\ &\quad - (\sin(\theta-\theta_1)/\sin(\theta_1-\theta_2))\, y_2(t) \end{aligned} \quad (2)$$

The instantaneous direction of the displacement vector in the horizontal plane is

$$\phi(\theta, t) = \tan^{-1}(y(\theta, t)/x(\theta, t)) \quad (3)$$

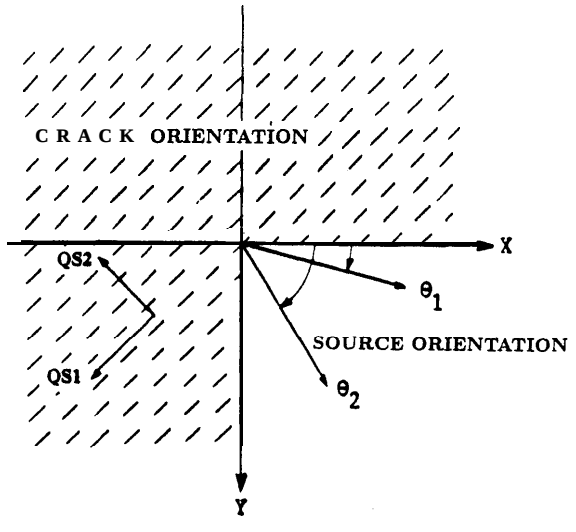

Fig. 1. Coordinate system and crack orientation in model structures.

where both $\phi(\theta, t)$, and θ are specified between 0° and 180°. $\phi(\theta, t)$ is sensitive to noise when x and y are small, and better signal-to-noise ratio is obtained by weighting each sample by its energy

$$E(\theta, t) = x^2(\theta, t) + y^2(\theta, t) \quad (4)$$

For a given source orientation θ, we sort the seismic energy in time interval $t_2 - t_1$ as a function of the displacement direction ϕ between 0° and 180°

$$F(\theta, \phi) = \sum_{t=t_1}^{t_2} E(t, \phi_k, \theta) \quad (5)$$

Where $E(t, \phi_k, \theta)$ is the seismogram energy at time t for direction ϕ in the interval $\phi_k - \Delta\phi \leq \phi \leq \phi_k + \Delta\phi$ for source orientation θ. $F(\theta, \phi)$ is evaluated for $0° \leq \theta \leq 180°$ in 1° steps, representing the full range of possible source orientations. $F(\theta, \phi)$ ranges over a square array of bins, where the elements correspond to the relative total energy associated with polarization direction ϕ as a function of source polarization.

We use two types of diagrams to show the variation of the energy as a function of polarization: 1) high-relief plots of $F(\theta, \phi)$, over the range of source orientations and displacement directions, and in which $F(\theta, \phi)$ is normalized and smoothed by averaging a square of 4 values, and 2) sums of energy, E, for each displacement direction ϕ for all calculated source orientations θ, which we plot as graphs against displacement directions

$$S(\phi) = \sum_{\theta=0°}^{180°} F(\theta, \phi) \quad (6)$$

3. PHYSICAL SIGNIFICANCE

Applying the processing described above, the data are transformed into the angular domain with two parameters: θ representing the source orientation; and ϕ representing the displacement direction in the horizontal plane. The energy of elastic wave-fields is proportional to the square of the amplitude, and the squared displacements for particular directions leads to the concept of polar energy. $F(\theta, \phi)$ of equation (5) can be characterized as a polar energy spectrum, which describes the properties of an elastic medium as a filter for transverse motion radiated from a horizontal source.

The distribution of total energy for isotropic media will be independent of direction and the distribution $F(\theta, \phi)$ will be unity for $\phi = \theta$ and zero for $\phi \neq \theta$. (Figure 4a is very close to isotropy as a delay between the split shear waves has not had time to develop at the shallow depth.) However, the distribution of polarization energy changes for propagation in an anisotropic medium. In the presence of anisotropy-induced shear wave splitting, when all possible source orientations are taken into account, the maxima of the polar energy spectrum $F(\theta, \phi)$ coincide with the polarizations of the split shear waves despite complicated particle motion.

This seismic analysis is analogous to optical experiments, where the intensity of initially linearly polarized light is measured as a function of polarization after propagation through specimens such as anisotropic crystals, or optically active solutions, which affect the initial polarization.

4. APPLICATION TO SYNTHETIC DATA

4.1. *Near-Vertical VSP's*

To illustrate the effect of anisotropy in distributing seismic energy in polarization directions related to the medium rather than the source, we analyze synthetic VSP data calculated with the ANISEIS modelling package which uses a modified anisotropic reflectivity technique [*Crampin*, 1987]. The model parameters of the anisotropic medium are given in Table 1. Using the formulations of *Hudson* [1980, 1981], we model the anisotropy of parallel vertical water-filled cracks striking 135° clockwise from the x direction. The crack density is 0.03, the aspect ratio of the cracks is 0.001 and the crack radius 1 mm. Ten geophones are aligned vertically below the source with a separation of 300 m. The top geophone is at a depth of 100 m. The dominant frequency of the horizontal point-force source pulse is 15 Hz. For near-vertical propagation the faster split shear wave, *qS1*, is polarized parallel, and the slower split shear wave, *qS2*, is polarized perpendicular to the strike of the cracks.

Figure 2 shows the horizontal components and the polarization diagrams in the horizontal plane of the shear wave arrivals in the horizontal plane for geophones 1 to 10 when the source polarization is in the x direction. The patterns of motion are characteristic of shear waves propagating through anisotropic media with increasing time delay for the longer ray paths. When the time delay is large enough (geophone 5 and below) visual identification of the polarization of the split shear waves in polarization diagrams is easy as the motion displays, either nearly cruciform linear components (geophones 8 to 10), or characteristic patterns of motion (geophones 5 to 7) from which the parameters may be estimated. However, for small delays, as at geophones 1 to 4, the particle motion is highly elliptical and it is difficult to identify the directions of the split shear waves with any reliability. The intermediate delays at geophones 5 to 7 result in constructive interference so that the maximum displacements are perpendicular to the initial source radiation [*Crampin*, 1978]. We test our processing techniques for these typical cases by applying the processing techniques to geophones 1, 6, and 10 in turn.

TABLE 1. Model VSP Parameters for Vertical Velocities

	Thickness, km	V_{qP}, km/s	V_{qS1}, km/s	V_{qS2}, km/s	ρ, g/cm^3
Isotropic half-space	∞	5.0	2.89	-	2.5

Figure 3 shows the distribution of polar energy for geophones 1, 6, and 10, from Figure 2. At geophone 1, for very small time delay, the energy is scattered about the polarization of the source, and the polarizations of the split shear waves, *qS1* and *qS2*, cannot be distinguished. At geophone 6, the constructive interference leads to a considerable amount of energy orthogonal to the source orientation. In addition, the two dominant peaks are complicated and do not exactly coincide with the polarization of *qS1* and *qS2*. For large delays as at geophone 10, the directions of *qS1* and *qS2* are clear and unambiguous. These results agree with what can be obtained by visual inspection of the polarization diagrams in Figure 2.

If we now calculate seismograms with a source oriented perpendicular to those in Figure 2, and linearly combine seismograms from orthogonal source orientations, we can calculate the distribution of polar energy $E(\theta, \phi)$ for a range of source polarizations θ between 0° and 180° and sort them into 1° bins of ϕ for $0° \le \phi \le 180°$. These polar energy spectra are shown in Figure 4 for geophones 1, 2, 6, and 10. When a source polarization is simulated that coincides with the polarization of either *qS1* or *qS2*, the particle motion is linear and the motion confined to this polarization direction. For any other source polarization, the energy is scattered into the polarization directions of the two split shear waves. This effect can be seen in Figure 4. The spikey nature of the peaks is caused by the sorting mechanism applied to a sampling rate of 2000 Hz (0.5 ms). For the very small time delay between the split shear waves at geophone 1 the linear combination shows that the recorded motion for any source polarization will mainly be polarized in this direction. It is already obvious that more energy is transmitted where the source orientation coincides with the *qS* polarizations. This becomes more distinct for increasing time delay. The maxima of the polar energy spectra correspond to the polarization directions of the split shear waves.

As a final processing step, in Figure 5 we plot S(f), the sum of the frequencies of the polar energy over all source orientations for each displacement direction. The polarization directions of *qS1* and *qS2* are dominant and there is very significant improvement over the diagrams in Figures 3*a* and 3*b*. In particular for the small time delays at geophone 1 and 2 the *qS* polarizations could be determined which was not possible by visual inspection. Figure 5 shows nicely the polarization filtering effect of anisotropic media.

4.2; Reflections From the Lower Crust

We now apply the processing techniques to a seismogram section from a synthetic shear wave reflection survey recording reflections from a laminated lower crust. The large number of interfering reflections of shear waves gives

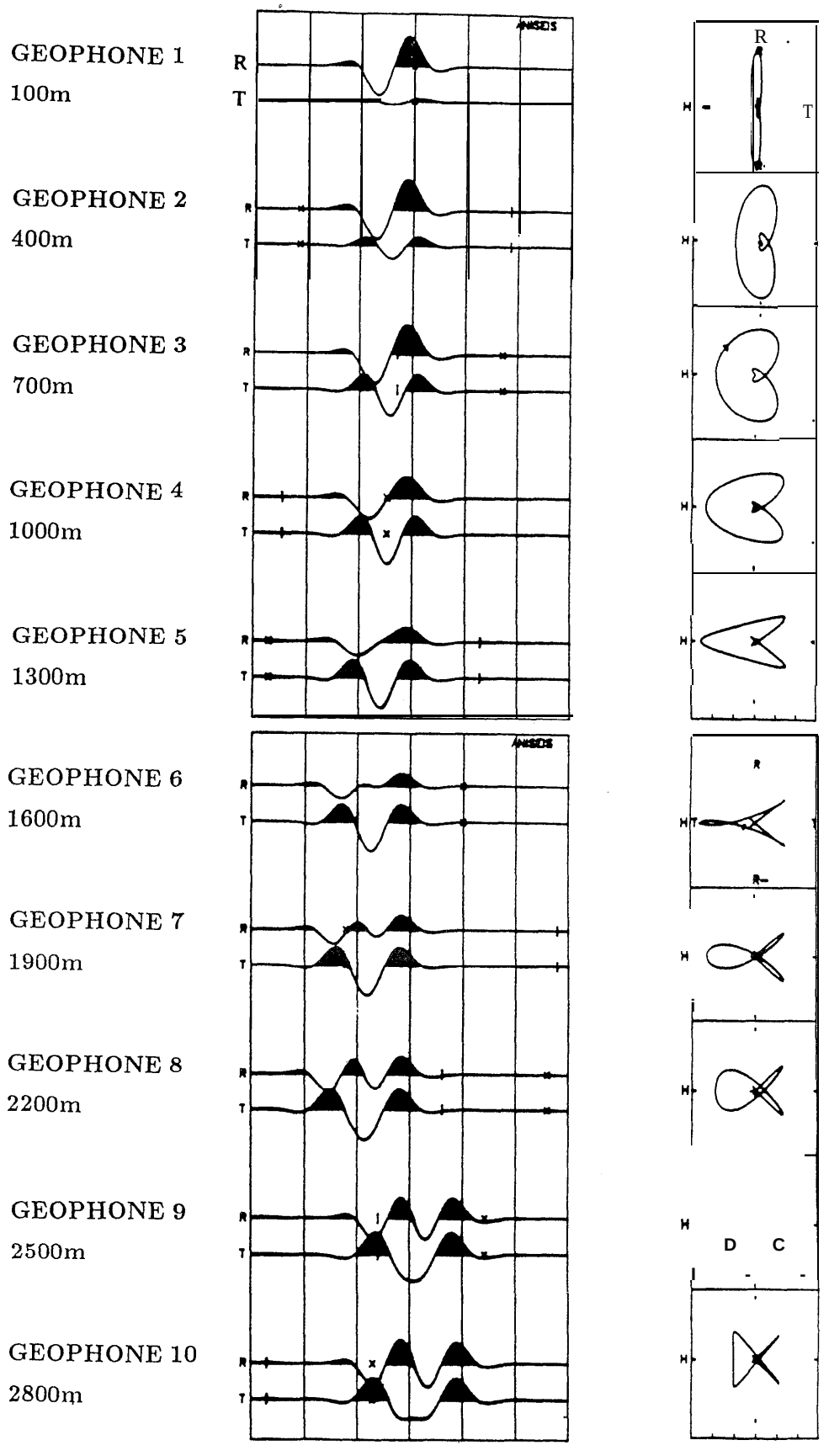

Fig. 2. Horizontal components and polarization diagrams of particle motion in the horizontal plane for seismograms from the VSP model described in Table 1, for geophones 1 to 10, with source polarized in x direction. Depth in metres is given. The directions are marked toward (T) and away from (T-) the source, and left (R-) and right (R) from the source.

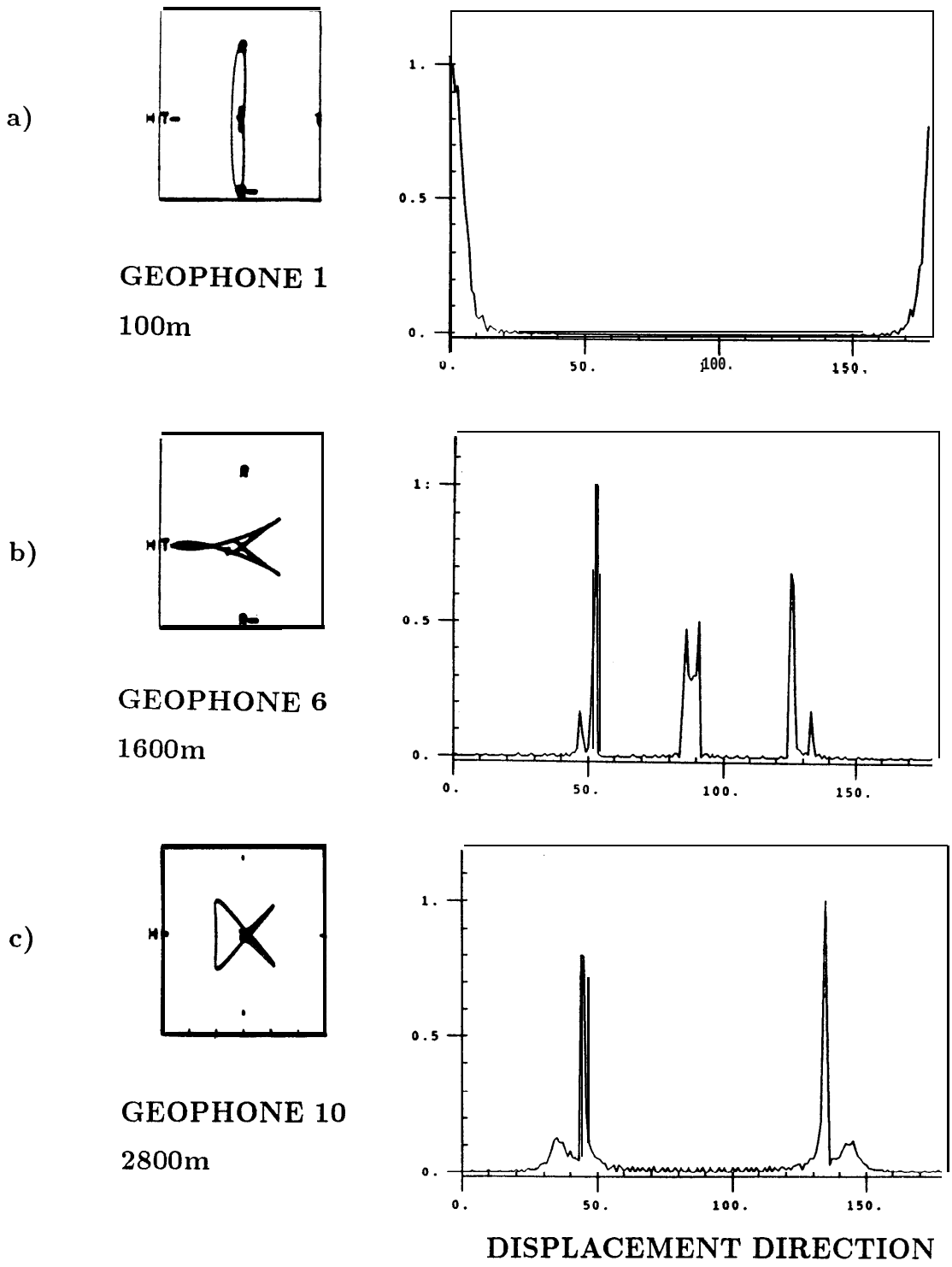

Fig. 3. The particle motion and distributions of displacement directions in the horizontal plane for geophones 1, 6, and 10, from the synthetic VSP survey for the structure in Table 1. Shear wave source aligned in x direction. (*a)* Geophone 1. (b) Geophone 6. (c) Geophone 10. Notation as in Figure 2.

strongly elliptical particle motion, which hides simple visual recognition of the polarization directions.

The continental lower-crust is strongly reflective in many parts of the world. ***Wentel et al.*** [1987] interpret the high *P* wave reflectivity in' the lower crust beneath the Black Forest in Germany as the result of alternating lamellae with Pwave velocities ranging from 5.5 to 7.5 km/sec and an average thickness of 120 m. Source and recording technology are now advanced enough to consider experiments designed to examine the

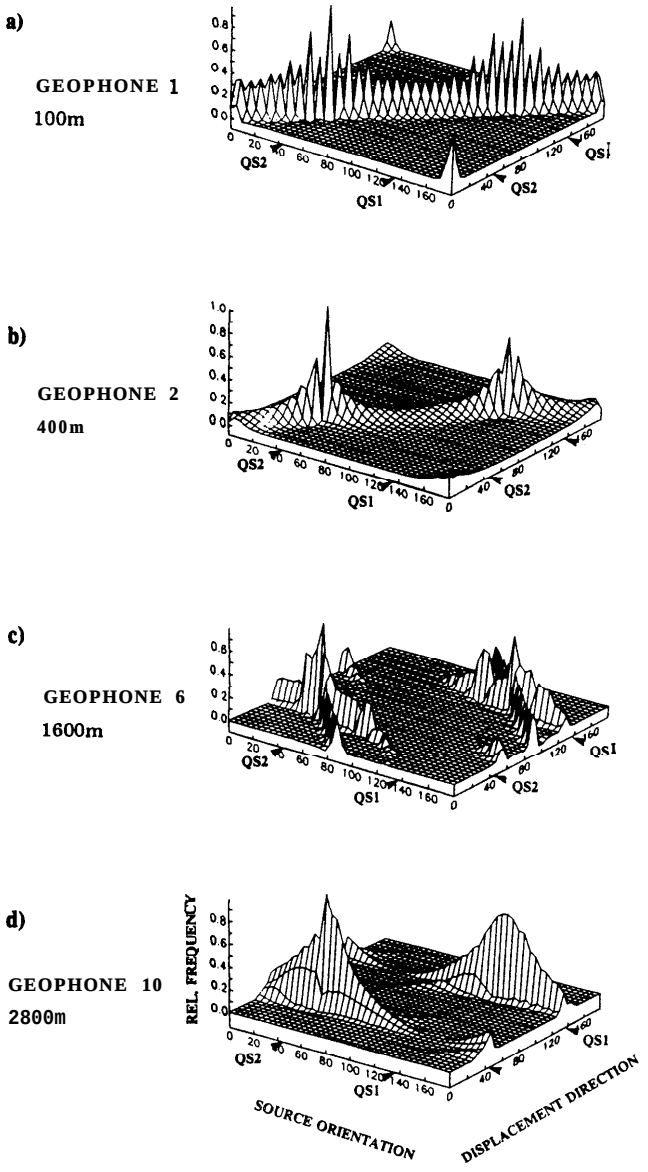

Fig. 4. Polar energy spectra, $F(\theta,\phi)$, for all source orientations for VSP mode, ranging over 180° of source orientations and 180° of displacement direction. (*a*) Geophone 1. (*b*) Geophone 2, (c) Geophone 6, and (*d*) Geophone 10.

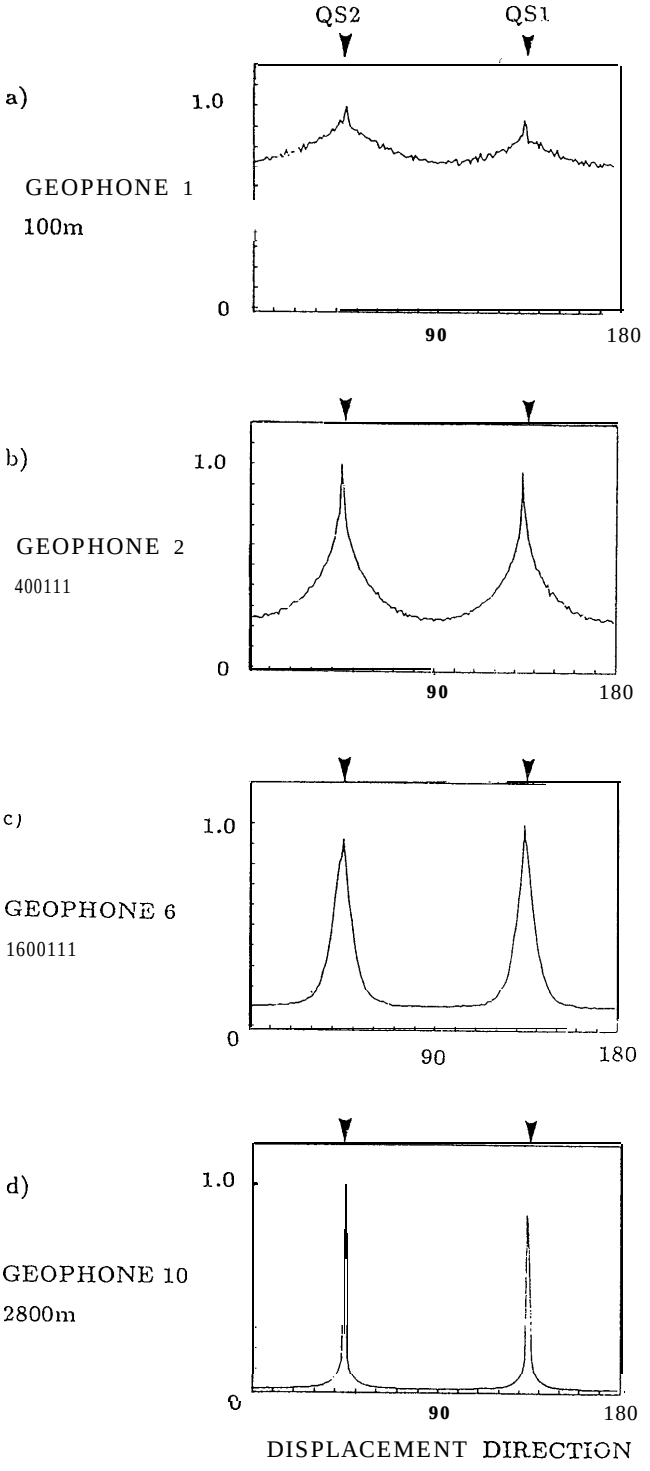

Fig. 5. Polar energy spectra summed over 180° of source orientation for each polarization direction for the same data as Figure 4.

behavior of shear wave reflections from the lower crust; several have been attempted, although the results are not yet available.

There is an increasing number of publications reporting shear wave recordings above small earthquakes, where the polarization of the faster split shear wave is parallel to the direction of maximum compressional stress. *Crampin and Booth* [1985] interpret this as the effect of extensive-dilatancy anisotropy. Such stress-aligned cracks in the upper crust would have a crucial effect on the behavior of shear waves reflected from the lower crust, and we examine possible effects by processing synthetic shear wave seismograms reflected from an isotropic laminated lower crust underlying an anisotropic upper crust. A transverse isotropy of the lower crust due to the lamination would not have an effect on vertical shear wave propagation since there is no shear wave splitting in the direction of the axis of rotational symmetry. Vertical cracks in the laminated structure aligned, as in the upper crust, would only introduce a further small delay of the split shear wave trains and not affect the results. The interference of reflections and

multiples leads to highly elliptical particle motion, where the shear wave polarizations are not easily recognized by existing techniques.

The model parameters for a reflective lower crust are given in Table 2. The 15 km thick upper crust is anisotropic, modelled by a distribution of thin parallel vertical water-filled cracks with crack density 0.02. The size and shape of the cracks are the same as in the synthetic VSP model. The cracks strike N135°E of the x direction, and the initial polarization of the faster split shear wave coincides with the strike of the cracks. The lower crust consists of 20 horizontal high/low velocity layers with thicknesses between 50 and 200 m (Table 2). The average thickness is 120 m, as suggested by *Wenze I* e *t* al. [1987]. Source and receiver are located at the surface with a 200 m offset in the positive x direction.

TABLE 2. Model Reflection Parameters for Vertical Velocities

	Thickness, km		V_{qP}, km/s	V_{qS1}, km/s	V_{qS2}, km/s	P? g/cm^3
Aniso-tropic layer	15		5.8	3.26	3.17	2.8
Alter-nating iso-tropic layers	aver-age* 120	(L)	5.5	3.175	-	2.8
		(H)	7.0	4.041	-	2.8

*Thicknesses in metres from top: H 200; L 145; H 80; L 40; H 95; . L 110; H 140; L 70; H 160; L 120; H 100; L 105; H 130; L 170.

Figure 6*a* shows the horizontal components and the polarization diagrams in the horizontal plane for a record section containing the lower crustal reflections for a source orientation in the x direction. Apart from the first arrivals of the reflected faster split shear wave and the last arrivals of the slower split shear wave, the particle motion is elliptical due to interfering orthogonally polarized reflections and multiple arrivals. Figure 6*b* shows the distribution of the weighted frequency for a single source orientation, $\theta = 0°$, for the indicated section. There is large scatter and the polarizations of the split shear waves are hidden.

Figure 6*c* shows a plot of the bin distribution, $F(\theta, \phi)$, against displacement polarizations and source polarization. We see again the characteristic features of shear wave anisotropy as described in the previous section. The energy is

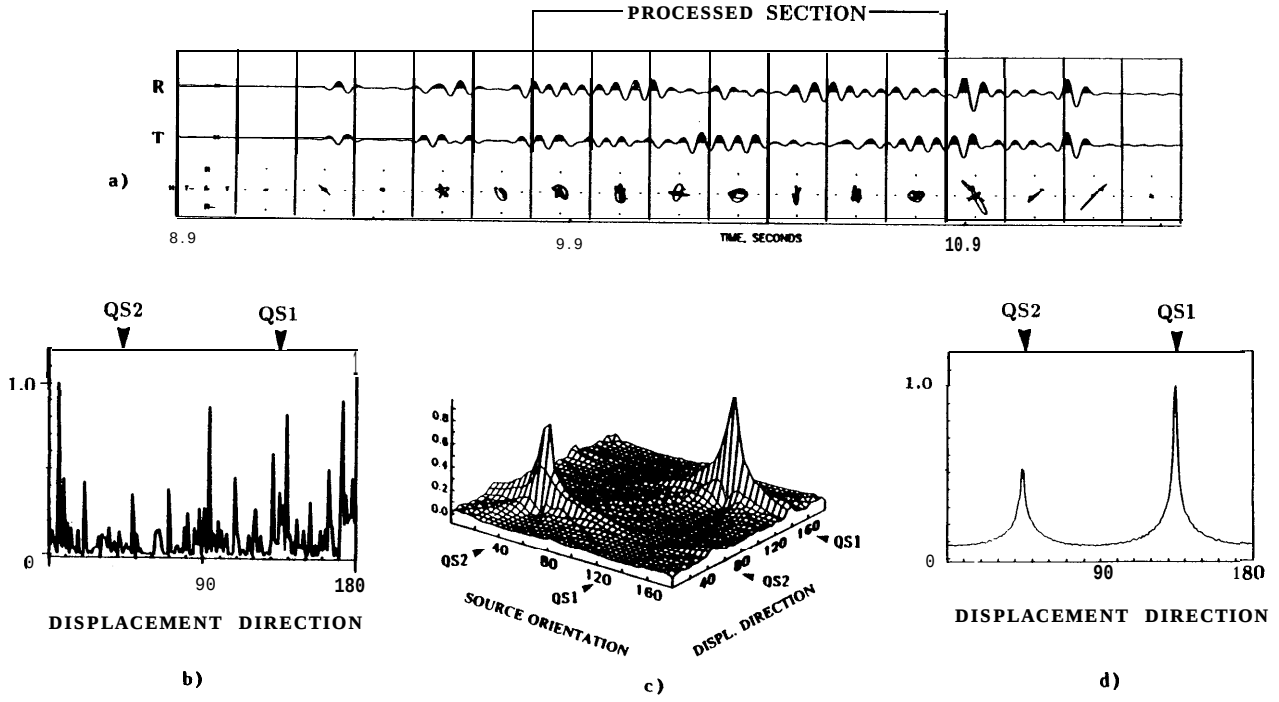

Fig. 6. (a) Horizontal components and particle motion diagrams in the horizontal plane for near-vertical reflections from a laminated lower crust. (6) Distribution of displacement directions for the seismogram section indicated in (a) for source in x direction. (c) Polar energy spectrum for the reflections from the lower crust indicated in (a) obtained by combining seismograms from two orthogonal polarizations. The maxima correspond to the crossover of the the polarization directions summed for each polarization angle for the example shown in (c), where the maxima are in the directions of the split shear waves *qS1* and *qS2*. (d) Summed polar energy spectra for data in (c).

concentrated where the source orientation coincides with the polarization of the split shear waves.

Summing the frequencies of the polarizations for all source orientations, $S(\phi)$, in Figure 6*d* shows the dominant effect of the polarization directions of the two split shear waves.

5. EXPERIMENTAL UNCERTAINTIES AND NOISE

Coherent and random seismic noise may have severe effects on the processing technique. We discussed the effects of internal interfaces and the free surface in the introduction. The effects of single internal interfaces are expected to be small [*Liu and Crumpin,* this issue], but the particle motion of surface recordings may be seriously disturbed by interaction with topographic irregularities. However, numerous numerical experiments show that the technique is stable when combining different source polarizations. For example, the same results are obtained, if the seismograms from one source polarizations are decreased (by up 40%, say), simulating different source strength, or a different directional response of the rock beneath the source. The results are also stable when seismograms from non-orthogonal source polarizations are combined, using the formulae for the orthogonal case (deviation $<\pm 30°$ from orthogonality), simulating uncertainty in the source orientation.

Different dominant frequencies of the source pulse (± 5 Hz) may have a large effect for small delays (at geophones 1 to 3) in the VSP survey (Figure 2). If the delays are large enough (below geophone 3), or we process a large number of overlapping arrivals (lower crust reflections), the dominant displacement directions still coincide with the *qS* polarizations. In order to test for the effects of noise, we contaminated each of the four horizontal seismogram components of both our synthetic examples needed for processing with independent random noise.

Examples of processed noisy signals are displayed in Figure 7. The quasi shear wave polarizations cannot be distinguished in the presence of more than about 5% noise for the very small time delays at geophone 1 in the VSP test in Figure 2. However, for small delays in geophones 2 and 3 in the VSP survey (Figure 7*a*), and the elliptical motion in the reflections from the lower crust (Figure 7*d*), the quasi shear wave polarizations can be distinguished for up to 30% random noise. For larger delays at geophones 4 and below in the VSP experiment, the polarizations are dominant for up to 50% noise (Figures 76 and c).

Low frequency noise has a large effect due to the long-period displacement of the origin from which the displacement direction is measured. We examined the effects of coherent linear and elliptical low frequency signals on the seismograms from two orthogonal sources. Note that 10% of linearly polarized low-frequency noise leads to dominant energy in the polarization direction of the noise for all geophones in the synthetic VSP survey. The effects are smaller if a large number of arrivals is processed as in the synthetic reflection and shifting of up to 15° for a signal-to-noise ratio <20%. Elliptically polarized noise may split the peaks and shift them up to 20° for noise <20%. It is important to note that the noise studies have been tested on synthetic seismograms with orthogonal source orientations. The effects of noise are expected to increase if nonorthogonal source orientations are used.

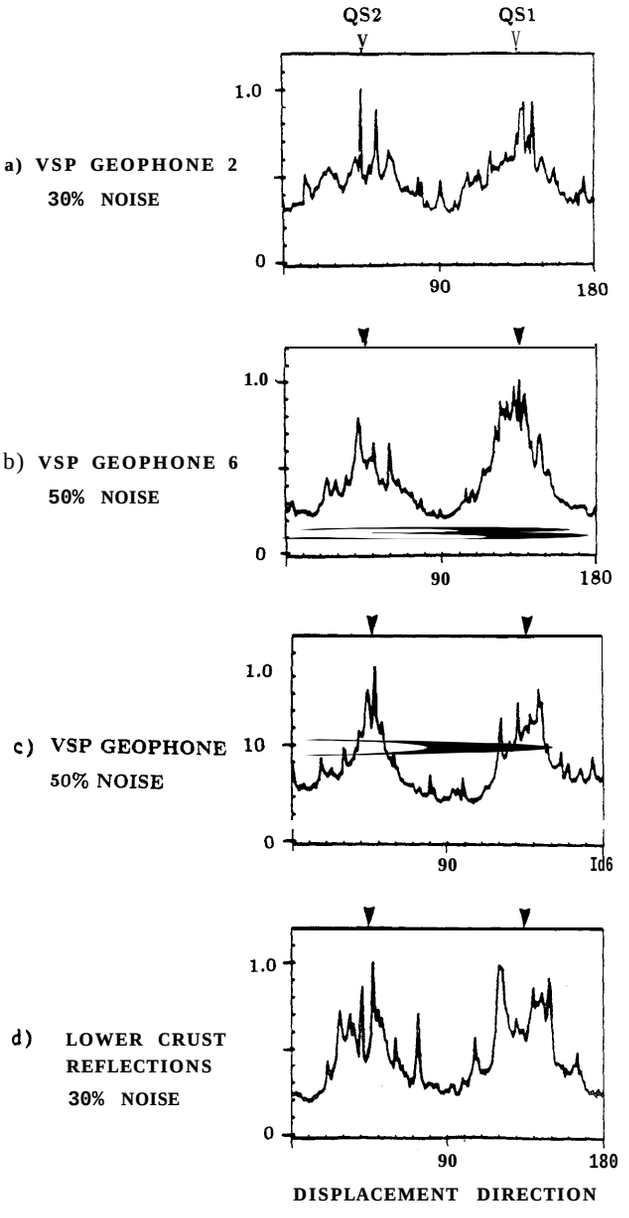

Fig. 7. Summed polar energy spectra as in Figures 5 and *6d* for the synthetic VSP survey in the presence of randomly oriented noise: (a) geophone 2 (30% noise); (*b*) geophone 6 (50% noise); and (c) geophone 10 (50% noise), and *(d)* lower crustal reflections (30% noise).

6. DISCUSSION

The visual interpretation of shear wave splitting is subjective, and several attempts have been made to extract information about shear wave splitting by automated processing of the displacements in the horizontal plane [*Naville,*

1986; *Nicoletis et al.,* 1988; *Shih et al.,* 1989]. Shih et al. determine the direction of the faster split shear wave by evaluating the linearity of the particle motion and relating maximum linearity to the polarization direction of the faster split shear wave. This method seems to work very well for shear wave recordings above small earthquakes where the time delays are large enough *[Savage et* al., this issue]. However, for small time delays with elliptical particle motion this method fails since the maximum linearity does not correspond to the polarization direction of the faster split shear wave.

Naville [1986] maximizes the correlation of the horizontal components of the shear wave recorded at different depths in a VSP survey, and relates the most symmetrical correlation to the principal directions of anisotropy. Naville assumes that the correlation is at right angles to the polarization direction, but again, this is only valid if the two split shear waves are separated sufficiently, and that the dominant particle motion is already in these directions.

The method of *Nicoletis et* al. [1988] diagonalizes a transfer matrix between two adjacent receivers in the frequency domain. This is an improvement since, expecially with small delays, manipulation of the frequency content in the low frequency domain can remove the ambiguities of the other two techniques, which fail if the particle motion is elliptical, by reducing the ellipticity with high-pass filtering. *Nicoletis et* al. [1988] point out that the measurement of the anisotropy is improved in quality and resolution if more than one source orientation is available, but do not attempt joint processing.

As seen in the previous sections, the effects of source orientation is crucial to the behavior of shear wave splitting. The information about the particle motion of any source orientation is contained in the response of the system to the two different source orientations, and can be used to determine the polarizations of the split shear waves. The maxima of the polar energy spectra may be expected to correspond to the axis of maximum horizontal compressional stress. However, it is important to note that vertical cracks in sedimentary basins in combination with the anisotropy of periodic sequences of thin layers do not necessarily yield polarizations parallel to the strike of the cracks throughout the shear wave window *[Bush and Crumpin,* 1987].

The advantage of the techniques suggested in this paper is that the actual particle motion of the single three-component seismogram is not important. The polarization response of the transmitting or reflecting medium for the full range of possible source polarizations echoes the inverse impedance of the propagation of the shear wave motion along the raypath, no matter how elliptical the particle motion. Since we are measuring from a fixed origin (zero displacement) the methods are sensitive to noise. The results depend on the quality of the data, in particular, the availability of records of different source polarizations.

7. CONCLUSIONS

Combining seismograms from different source polarizations allows the distributions of polarization directions to be correlated with the orientations of the split shear wave arrivals. In near-vertical VSPs and reflection surveys this may help to extract shear wave polarizations from data, which may be inaccessible by conventional techniques. The results may be largely independent of the time delay between the split shear waves, and may be particularly useful when the time delay is small or the motion is highly elliptical, when existing methods are likely to fail.

The synthetic examples we have discussed are for small offsets. The technique is valid for any offset and any plane of displacement approximately perpendicular to the propagation direction as long as there is substantial shear wave energy excited in the plane transverse to the raypaths for different source polarizations.

Acknowledgments. We thank Applied Geophysical Software Inc. and Macroc Ltd for approval to use the ANISEIS package for calculating the synthetic seismograms, and we are grateful to David C. Booth for his comments on the manuscript. This work was supported by the Natural Environment Research Council and is published with the permission of the Director of the British Geological Survey (NERC).

REFERENCES

Booth, D. C., and S. Crampin, Shear-wave polarizations on a curved wavefront at an isotropic free-surface, *Geophys. J. R. Astron. Soc., 83,* 31-45, 1985

Bush, I., and S. Crampin, Observations of EDA and PTL anisotropy in shear-wave VSPs, *Expanded Abstracts, 57th Annu. Int. Meeting,* pp. 646-649, Society of Exploration Geophysicists, New Orleans, La., 1987.

Cormier, V. F., The polarizations of S-waves in a heterogeneous isotropic Earth model, *J. Geophys., 56,* 20–23, 1984.

Crampin, S., Seismic wave propagation through a cracked solid: polarization as a possible dilatancy diagnostic, *Geophys. J. R. Astr. Soc., 53, 467-496, 1978.*

Crampin, S., Crack porosity and alignment from shear-wave VSPs, in *Shear-Wave Exploration,* vol. I, editored by S. H. Danbom and S. N. Domenico, *Geophysical Developments,* pp.227–251, Society of Exploration Geophysicists, Tulsa, Okla., 1987.

Crampin, S., and D. C. Booth, Shear-wave polarizations near the North Anatolian fault, II, Interpretation in terms of crack-induced anisotropy, *Geophys. J. R. Astron. Soc.,* 83, 75-92, 1985.

Douma, J., and K. Helbig, What can shear-waves tell us?, *First Break. 5, 3, 1987.*

Evans, J. R., Effects of free surface on shear-waves, *Geophys. J. R. Astron. Soc., 76,* 165-172, 1984.

Hudson, J. A., Overall properties of a cracked solid, *Math. Proc. Cambridge Philos. Soc., 8, 371-384,* 1980.

Hudson, J. A., Wave speeds and attenuation of elastic waves in material containing cracks, *Geophys. J. R. Astron. Soc.,* 64. 133-150, 1981.

Liu, E., and S. Crampin, Effects of the internal shear-wave window: comparison with anisotropy-induced splitting, *J. Geophys. Res.* , this issue.

Naville, C., Detection of anisotropy using shear-wave splitting in VSP surveys: requirements and applications, *Expanded Abstracts, 56th Annu. Int. Meeting,* pp. 391-394, Society of Exploration Geophysicists, Houston, Tex., 1986.

Nicoletis, L., C. Client, and F. Leveuvre, Shear-wave splitting measurements from multishot VSP data, *Expanded Abstracts, 58th Annu. Int. Meeting, I* . pp. 527-530, Society of Exploration Geophysicists, Anaheim, Calif., 1988.

Nuttli, O., The effect of the Earth's surface on the *S*-wave particle motion, *Bull. Seisol. Soc. Am.* . **44,** 237–246, 1961.

Nuttli, O., The determination of S-wave polarization angles for an Earth model with crustal layering, *Bull. Seismol Soc.* Am. , **54.** 1429-1440, 1964.

Shih, X. R., R. P. Meyer, and J. F. Schneider, An automated analytic method to determine shear-wave splitting, *Tectonophysics*, *165*, 271-278, 1989.

Savage, M. K., U. A. Peppin, and U. R. Vetter, Shear wave anisotropy and stress direction in and near Long Valley Caldera, California, 1979-1988, *J. Geophys. Res.*, this issue.

Wenzel, F., K.-J. Sandmeier, and W. Waelde, Properties of the lower crust from modelling refraction and reflection data, *J. Geophys. Res.*, *92*, 11,575-11,583, 1987.

S. Crampin, British Geological Survey, Murchison House, West Mains Road, Edinburgh EH9 3LA, Scotland, United Kingdom.

H. Igel, Institut de Physique du Globe, 4 place Jussieu, 252 Paris Cedex 05, France.

(Received January 31, 1989;
revised January 19, 1990;
accepted January 21, 1990.)